Precambrian Research 383 (2022) 106891

Contents lists available at ScienceDirect

Precambrian Research

journal homepage: www.elsevier.com/locate/precamres

CO_2 buildup drove global warming, the Marinoan deglaciation, and the genesis of the Ediacaran cap carbonates

Ruiyang Sun [a,b], Jun Shen [c], Stephen E. Grasby [d], Jiawei Zhang [e], Jianshu Chen [e], Chuang Yang [a,b], Runsheng Yin [a,*]

[a] State Key Laboratory of Ore Deposit Geochemistry, Institute of Geochemistry, Chinese Academy of Sciences, Guiyang 550081, China
[b] University of Chinese Academy of Sciences, Beijing 100049, China
[c] State Key Laboratory of Geological Processes and Mineral Resources, China University of Geosciences, Wuhan 430074, China
[d] Geological Survey of Canada, Calgary Natural Resources Canada, 3303 33rd Street NW, Calgary, AB T2L 2A7, Canada
[e] Guizhou Geological Survey, Bureau of Geology and Mineral Exploration and Development of Guizhou Province, Guiyang 550081, China

ARTICLE INFO

Keywords:
Cap carbonates
Early Ediacaran
Marinoan deglaciation
Mercury
Hg isotopes

ABSTRACT

What caused ocean/climate changes that drove Marinoan deglaciation, and the subsequent genesis of Ediacaran cap carbonates remains unclear. To address this issue, we examined the Hg records in Ediacaran cap carbonates from shelf to slope depositional settings in exposures from South China. These cap carbonates show higher total Hg (THg) concentrations (4.9 to 405 ppb), most of which are comparable to that observed in carbonates deposited during non-LIPs periods. The lack of THg/TOC anomalies in these cap carbonates suggests that background volcanic activity, rather than a short-term large igneous province event, drove the Marinoan deglaciation. The cap carbonates show positive Δ^{199}Hg values (0.18 to 0.34 ‰) in slope settings and slightly negative to slightly positive Δ^{199}Hg values (−0.16 to 0.11 ‰) in shelf settings, suggesting a binary mixing of seawater- and terrestrial-derived Hg in early Ediacaran Ocean. We infer that the accumulation of greenhouse gases, due to ongoing volcanic emissions of CO_2 and enhanced release of gas hydrates, triggered global warming. This warming led to melting of sea ice cover, enhanced terrestrial inputs of alkalis (e.g., K^+, Na^+, Ca^{2+}, Mg^{2+}), and large-scale dissolution of atmospheric CO_2 into seawater, driving widespread deposition of Ediacaran cap carbonates.

1. Introduction

Cap carbonates, that are meter- to decameter-thick dolostone or limestone layers overlying Marinoan glacial diamictites (Hoffman et al., 2017), represent the abrupt termination of the Marinoan Ice Age at *ca.* 635 Ma (Condon et al., 2005; Yu et al., 2020). These cap carbonates are characterized by negative carbon isotope ($\delta^{13}C$) excursions reflecting profound changes in ocean chemistry soon after the Cryogenian glaciation (Wang et al., 2008; Sansjofre et al., 2011); which may have an important connection to oceanic/atmospheric oxygenation (Lang et al., 2018) and the early evolution of complex multicellular eukaryotes in the following Ediacaran period (Zhao et al., 2021).

The formation of cap carbonates was associated with sea-level rise during the Marinoan deglaciation (Fairchild et al., 2016) and has been interpreted by multiple models, including the upwelling of alkalinity-rich deep-ocean seawater (Knoll et al., 1996), postglacial chemical weathering of silicate and carbonate rocks (Hoffman et al., 2017; Myrow et al., 2018), oxidation of methane from gas hydrate destabilization (Jiang et al., 2006; Kennedy et al., 2008), and microbially mediated carbonate precipitation from deglacial meltwater (Shields, 2005). In each of these models, changes in ocean chemistry during the Marinoan deglaciation could provide a favorable environment for cap carbonates deposition, such as high alkalinity (Hoffman, 2011) and enhanced biotic activity (Meyer et al., 2012).

The ultimate driving force for the Marinoan deglaciation remains unclear but has been linked to global warming driven by rising greenhouse gas (e.g., CO_2) levels in the atmosphere (Hyde et al., 2000; Kennedy et al., 2001). Events such as large igneous provinces (LIPs) eruptions, can lead to transient emissions of large amounts of CO_2 to the atmosphere. When LIPs are absent, background volcanism could also cause a slow accumulation of CO_2 in the atmosphere if normal processes of CO_2 drawdown are inhibited. We examine these two possibilities here

* Corresponding author.
E-mail address: yinrunsheng@mail.gyig.ac.cn (R. Yin).

https://doi.org/10.1016/j.precamres.2022.106891
Received 7 July 2022; Received in revised form 24 October 2022; Accepted 25 October 2022
Available online 8 November 2022

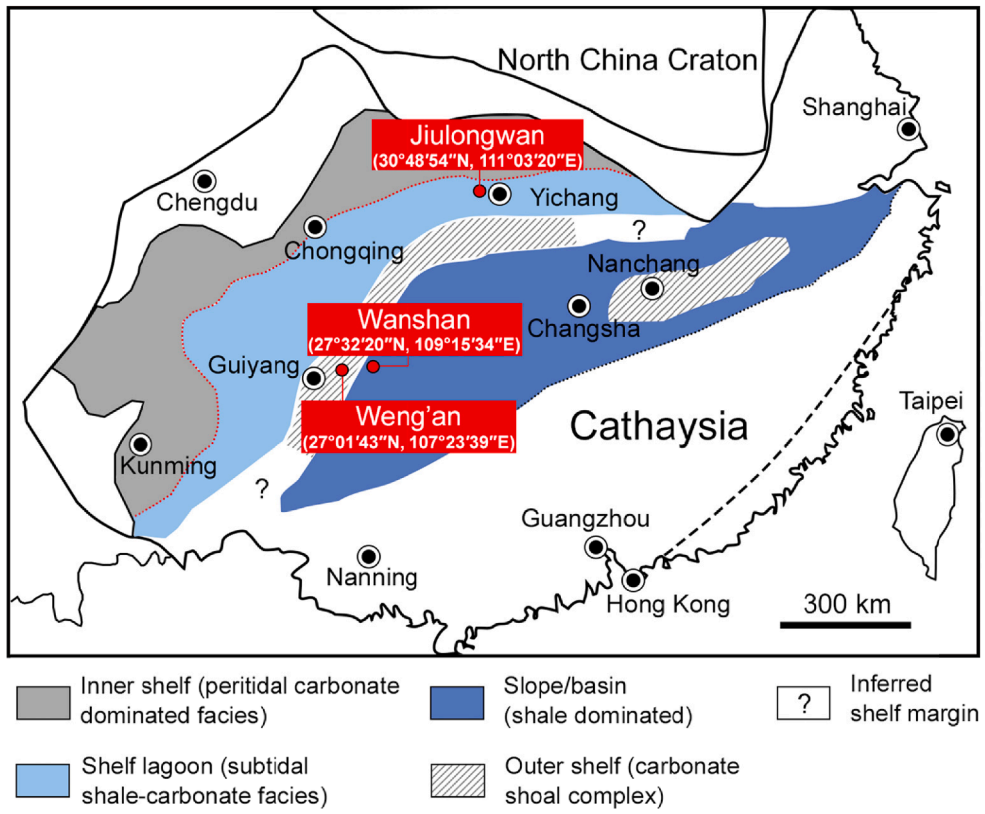

Fig. 1. Geological map showing the paleogeography of the Yangtze platform during the Ediacaran Doushantuo deposition and the location of sampling sites (Modified from Jiang et al., 2011).

using mercury (Hg) as a proxy.

Mercury (Hg), a highly volatile metal, is capable of tracing volcanism through geological history (Grasby et al., 2019) as LIP events transiently emit large amounts of Hg (Sanei et al., 2012; Grasby et al., 2020). This Hg is mainly in gaseous Hg(0) form that is transported globally in the atmosphere before depositing into terrestrial and marine systems (Selin, 2009), resulting in anomalously high Hg concentrations in sediments. Owing to the affinity of Hg to organic matter, anomalous high Hg to total organic carbon (Hg/TOC) ratios in sediments can better reveal large volcanic eruptions (Grasby et al., 2019). Other potential drawdown mechanisms have to be excluded though, as well as using isotope systems to ascribe a Hg source. Mercury isotopes undergo mass-dependent fractionation (MDF, defined as δ^{202}Hg) and unique mass-independent fractionation (MIF, defined as Δ^{199}Hg). Hg-MDF occurs ubiquitously during physical, chemical, and biological processes, therefore δ^{202}Hg is not easily used as a Hg source tracer (Kwon et al., 2020). Volcanic Hg usually has Δ^{199}Hg ~ 0 (Zambardi et al., 2009), but photochemical processes in the surface environment can alter this signal, resulting in positive Δ^{199}Hg in marine systems (e.g., seawater and marine sediments) and negative Δ^{199}Hg in terrestrial systems (e.g., soil and vegetation) (Blum et al., 2014). The Hg-MIF signatures are not altered by sedimentation and diagenesis processes, therefore, Δ^{199}Hg can be used to constrain Hg sources in sediments (Grasby et al., 2019). Recent studies have reported Hg (or Hg/TOC) anomalies with significant Δ^{199}Hg shifts during the Cryogenian interglacial greenhouse (Zhou et al., 2021), end-Permian mass extinction (Grasby et al., 2017; Shen et al., 2019a, 2019b) and Triassic-Jurassic (*T*-J) mass extinction (Thibodeau et al., 2016), highlighting LIP eruptions as drivers of these events. However, Hg records of the Marinoan deglaciation have not been well explored.

Sections of Ediacaran cap carbonates are widely distributed in the Yangtze Platform, South China. Here, we investigate Hg concentration and isotopic composition, trace elements, and TOC content of cap carbonates deposited in different depositional settings in the Yangtze Platform, to gain an understanding of the cause of the Marinoan deglaciation and the mechanisms of cap carbonate formation.

2. Geological background

During the breakup of supercontinent Rodinia, a passive continental margin was formed on the southeastern edge of the Yangtze Platform, providing favorable conditions for Neoproterozoic sedimentation (Fig. 1, Jiang et al., 2003). The Neoproterozoic succession in the Yangtze Platform consists of three lithostratigraphic units, the Tonian unit consisting of siliciclastic rocks, the Cryogenian glacial-interglacial unit consisting of mixed deposition of siliciclastic rocks and glacial diamictites, and the Ediacaran unit consisting of mixed deposition of carbonate and siliciclastic rocks. The upper part of the Cryogenian glacial sequence (Nantuo Formation) consists of glacial diamictites and corresponds to the Marinoan Ice Age deposition (Jiang et al., 2003; Zhou et al., 2019). The lower part of the Ediacaran Doushantuo Formation lies over the Nantuo Formation (Jiang et al., 2011) and consists of cap carbonates, which are predominantly composed of massive dolostones with typical sedimentary structures, such as tepees, crossbedding, and rip-up clasts (Shields, 2005). During the Early Ediacaran the Yangtze Platform can be divided, from northwest to southeast, into shelf, slope, and basin depositional settings (Fig. 1). The Doushantuo cap carbonates are observed in the shelf and slope settings.

The Hg data of the Ediacaran cap carbonates (n = 6) was recently reported from the inner shelf setting of the Jiulongwan section (Fig. 2, Fan et al., 2020). To identify if the Hg isotope pattern observed is of broader significance, two sections in the Yangtze Platform (Fig. 1), including the Weng'an section (27°01′43″N, 107°23′39″E) from the outer shelf setting and the Wanshan section (27°32′20″N, 109°15′34″E) from the slope setting, were sampled in this study. In these sections, the Doushantuo cap carbonates are well exposed (Jiang et al., 2011). As

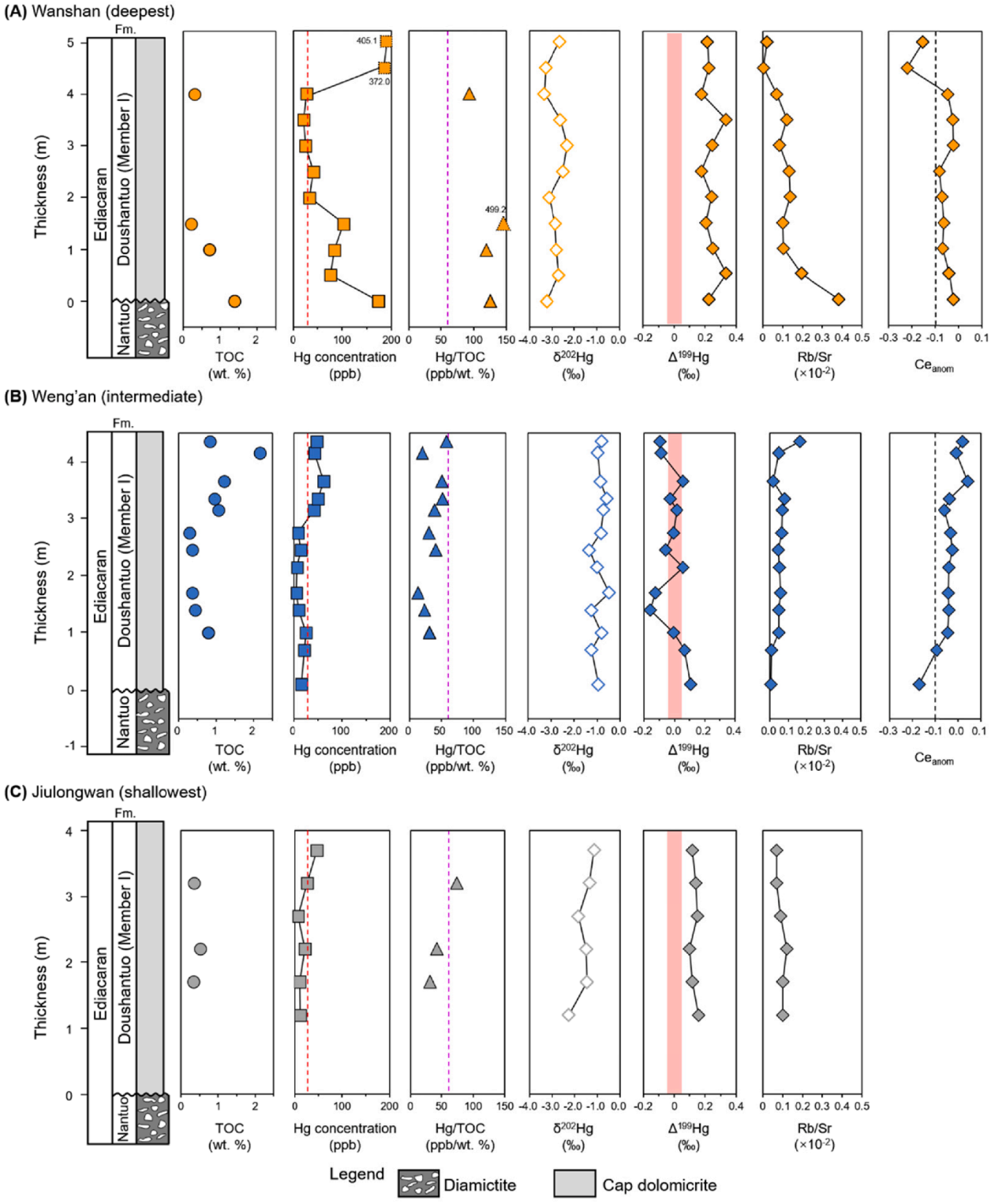

Fig. 2. TOC concentrations, Hg concentrations, Hg/TOC ratios, δ^{202}Hg, Δ^{199}Hg, Rb/Sr ratios, and Ce_{anom} values of (A) the Wanshan section, (B) the Weng'an section, and (C) the Jiulongwan section (after Fan et al. (2020)). The red dashed line represents the mean value for Hg in carbonates (28.3 ± 91.9 ppb) and the purple dashed line represents the mean value for Hg/TOC ratios of ancient carbonates during non-LIPs periods (59.5 ± 86.5 ppb/wt.%). The red bars represent the Δ^{199}Hg of the volcanic Hg (0 ± 0.05 ‰, Zambardi et al., 2009). The black dashed lines mean the redox boundary of the Ce_{anom} value (−0.1). TOC concentrations and Hg/TOC ratios have not been involved for samples with TOC content lower than 0.2 wt%. The data of the Jiulongwan section are from Fan et al. (2020). Fm = Formation.

shown in Fig. 2, the Wanshan and Weng'an sections contain glacial diamictites in the upper part of the Nantuo Formation (~1 m), and cap dolostones in the Doushantuo Formation Member I (~5 m), similar to the Jiulongwan section.

3. Methods

Ediacaran cap carbonates were sampled from the Wanshan (n = 11) and Weng'an (n = 13) sections (Fig. 1). The samples were trimmed to

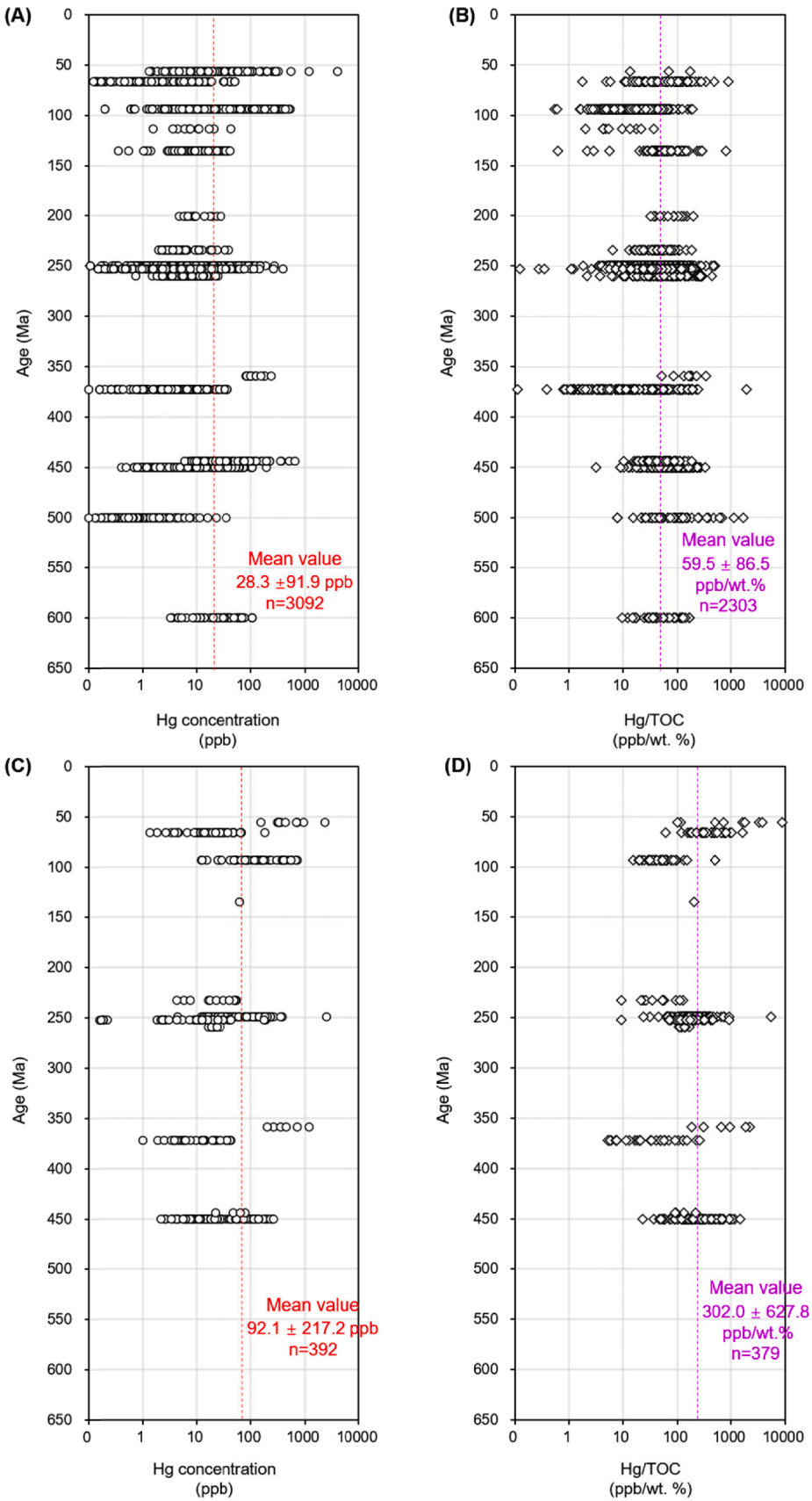

Fig. 3. Plots of (A) Hg concentrations and (B) Hg/TOC values for ancient carbonates during non-LIPs period and plots of (C) Hg concentrations and (D) Hg/TOC values for ancient carbonates during LIPs period. The dashed lines represent the mean values. Data source: see Supplementary **Table S3** and references therein.

remove weathered surfaces, pulverized to ~ 200 mesh, and homogenized before chemical analyses at the Institute of Geochemistry, Chinese Academy of Sciences.

For total organic carbon (TOC) analyses, the sample powders were acidified using 2 M HCl to remove the carbonate fraction. After centrifuging, the residual samples were washed thrice using deionized purified water. After washing, the residual samples were analyzed for total carbon, representing the TOC fraction. TOC concentrations in sediment samples were measured using the potassium dichromate oxidation spectrophotometric method (detection limit: 0.1 wt%, Schumacher, 2002). Trace elements (e.g., Rb, Sr, and rare earth elements) were measured by an Agilent 8900 inductively coupled plasma mass spectrometry (ICP-MS), following the procedures of Liang et al. (2000). The analytical uncertainty for trace elements was better than ± 5 % based on the long-term results of two reference materials (carbonate, COQ-1; shale, SBC-1).

Total Hg (THg) concentration was measured using a Lumex RA-915F Hg analyzer (detection limit: 0.05 ng/g). About 350 mg of samples were used in this analysis. Results were calibrated to the standard reference material (SMR) GSS-5 (soil, 290 ppb). One replicate and a standard were analyzed every-five samples. Data quality was monitored via multiple analyses of standard GSS-5, yielding an analytical precision of 90–110 % for GSS-5 and uncertainty of < 10 % (2SD) for triplicate samples.

Hg in sedimentary samples was preconcentrated into 5 mL of 40 % anti aqua regia ($HNO_3/HCl = 2/1$, v/v) using a double-stage combustion method developed for Hg isotope analysis (see more details in Zerkle et al., 2020). After the preconcentration, the trapping solution was diluted to 1 ppb Hg and the highest acid concentration of ~ 20 %, for the analysis using a Neptune Plus multi-collector-inductively coupled plasma mass spectrometer (MC-ICP-MS), following the method by Yin et al. (2016). Standard reference material (GSS-4, soil) was prepared in the same way as the samples. Hg concentrations and acid matrices in the bracketing National Institute of Standards and Technology 3133 (NIST-3133) solutions were matched well with the neighboring samples. Mercury isotopic compositions were reported following Blum and Bergquist (2007). MDF is expressed in δ^{202}Hg notation in units of permil (‰) referenced to the NIST-3133 Hg standard:

$$\delta\,^{202}Hg(‰) = \left[\left(\,^{202}Hg/\,^{198}Hg_{sample}\right)/\left(\,^{202}Hg/\,^{198}Hg_{standard}\right) - 1\right] \times 1000 \quad (1)$$

MIF is reported in Δ notation, which describes the difference between the measured δ^{xxx}Hg and the theoretically predicted δ^{xxx}Hg value, in units of ‰, with xxx = 199, 200, or 201:

$$\Delta\,^{xxx}Hg = \delta\,^{xxx}Hg - \delta\,^{202}Hg \times \beta \quad (2)$$

β equals to 0.2520 for ^{199}Hg, 0.5024 for ^{200}Hg, and 0.7520 for ^{201}Hg (Blum and Bergquist, 2007). Analytical uncertainty was estimated based on the replicates of the NIST-3177 secondary standard solution and full procedural analyses of SRM GSS-4 (soil). The overall average and uncertainty of NIST-3177 (δ^{202}Hg: −0.50 ± 0.10 ‰; Δ^{199}Hg: −0.01 ± 0.03 ‰; Δ^{200}Hg: 0.02 ± 0.04 ‰; Δ^{201}Hg: 0.01 ± 0.04 ‰, 2SD, n = 6) and GSS-4 (δ^{202}Hg: −1.53 ± 0.10 ‰; Δ^{199}Hg: −0.44 ± 0.05 ‰; Δ^{200}Hg: −0.02 ± 0.08 ‰; Δ^{201}Hg: −0.37 ± 0.06 ‰, 2SD, n = 3) agree well with previously reported studies (Blum and Bergquist, 2007; Deng et al., 2021). The larger 2SD values of either NIST-3177 or GSS-4 are used to reflect analytical uncertainties.

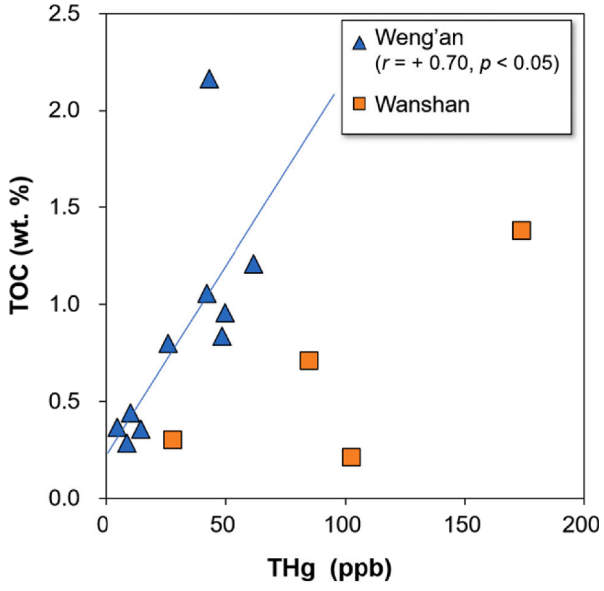

Fig. 4. The relationship between THg concentration and TOC content in the studied sections.

4. Results

Hg concentrations, isotopic compositions, and TOC contents of Ediacaran cap carbonates in the two studied sections are shown in **Table S1** and Fig. 2. In the Wanshan section (Fig. 2**A**), the samples show low TOC contents (0.65 ± 0.53 wt%, SD), and some are even lower than the detection limit (0.1 wt%). The samples have large variation in THg concentrations (4.9 to 405 ppb) and Hg/TOC ratios (93.7 to 499 ppb/wt.%). Only samples with TOC values > 0.2 wt% are calculated and plotted in Fig. 2**A** to avoid error (Grasby et al., 2019). In the Weng'an section (Fig. 2**B**), the samples show slightly higher TOC contents (0.85 ± 0.57 wt%, SD), but obviously lower Hg concentrations (4.9 to 61.8 ppb) and Hg/TOC ratios (lower than 60 ppb/wt.%) than the Wanshan section.

Negative δ^{202}Hg values are observed in the Wanshan section (−3.34 to −2.32 ‰) and Weng'an section (−1.34 to −0.48 ‰). In the Wanshan section (Fig. 2**A**), positive Δ^{199}Hg values are observed (0.18 to 0.34 ‰). In the Weng'an section (Fig. 2**B**), the Δ^{199}Hg shows positive values (0.11 ‰) at the bottom of the section, and then show a shift toward negative values (−0.10 ‰) at the top of cap carbonates. There is then a positive excursion in the Δ^{199}Hg values from −0.16 ‰ to 0.06 ‰, followed by a return to negative values in the upper part of the section.

Concentrations of redox-sensitive elements are listed in **Table S2**. The Ce anomalies (Ce_{anom}) are calculated by formulae: $Ce_{anom} = Lg(3 \times Ce_N/(2 \times La_N + Nd_N))$ (Haskin et al., 1968; Tylor and McLennan, 1985). Elements with subscript N represent the concentration normalized to Post-Archaean Australian Shale (PAAS, McLennan, 1989). The Wanshan and Weng'an cap carbonate samples sections show negative Ce_{anom} values of −0.07 ± 0.06 (SD) and −0.04 ± 0.05 (SD), respectively). The Rb/Sr ratios in the Wanshan section (0.15 ± 0.10, SD) are higher than the Weng'an section (0.06 ± 0.05, SD).

Results in this study are partially different from previous results of the cap carbonates in the Jiulongwan section (Fig. 2**C**, Fan et al., 2020). Cap carbonates in the Jiulongwan section show similar TOC contents (0.40 ± 0.10 wt%, SD), Hg concentrations (7.9 to 46.5 ppb), and Hg/TOC ratios (32 to 74 ppb/wt.%) to the Wanshan and Weng'an sections. The Jiulongwan section is also characterized by negative δ^{202}Hg (−2.25 to −1.13 ‰) and positive Δ^{199}Hg values (0.10 to 0.16 ‰) (Fig. 2**C,** Fan et al., 2020). Δ^{199}Hg shows a shift toward less positive values in the Jiulongwan section, similar to the trend in the Weng'an section, but with a steadier decline. Overall, the Weng'an section shows the lowest Hg concentrations and Hg/TOC ratios, and the Wanshan section shows the most positive Δ^{199}Hg values amongst these three sections.

5. Discussion

5.1. Mercury host phases in Ediacaran cap carbonates

The large volume of data produced over the last several years provides great insight into Hg in carbonates in the geologic record. We have

examined previous studies on Hg in carbonates and sorted out the Hg concentrations and Hg/TOC ratios of ancient carbonates (see **Table S3** and references therein). These studies found Hg enrichment in carbonates at boundaries related to LIPs eruptions, but low Hg concentrations in carbonates below or above these Hg-rich boundaries (Fig. 3). Based on previous results on carbonates deposited during non-LIPs periods, we propose a background Hg value of 28 ± 92 ppb (SD, n = 3092, Fig. 3**A**) and a background Hg/TOC ratio of 60 ± 43 ppb/wt.% (SD, n = 2303, Fig. 3**B**) for non-LIPs carbonates (Meyer et al., 2019; Tremblin et al., 2022; Font et al., 2016, 2021; Sial et al., 2013, 2016; Scaife et al., 2017; Benigno et al., 2021; Charbonnier et al., 2017; Percival 21et al., 2015; Thibodeau et al., 2016; Zhao et al., 2022a, 2022b; Shen et al., 2019a, 2019b; Kailho et al., 2020; Wang et al., 2018; Grasby et al., 2017; Hu et al., 2021; Huang et al., 2018; Rakociński et al., 2021; Zhang et al., 2021; Racki et al., 2018, 2020; Jones et al., 2017; Gong et al., 2017; Pruss et al., 2019; Fan et al., 2020). In this study, Hg concentrations in Ediacaran cap carbonates show the 16th to 84th percentile range of 10.5 to 76.8 ppb, which are comparable to previous results on carbonates deposited during non-LIPs periods, according to the lack of statistical difference through *t*-test analysis (t = 1.924, p = 0.064). Mercury potentially occurs in marine sediments as organic-bound, clay-bound, and sulfides species (Sanei et al, 2012; Shen et al., 2020). As shown in Fig. 4, significant positive correlations between THg and TOC can be observed in Ediacaran cap carbonates in the Weng'an (r = + 0.70, p < 0.05) section, suggesting that Hg is mainly hosted in organic matter in the Weng'an section.

5.2. Lack of large-scale volcanic eruption of short-term duration during the Marinoan deglaciation?

Anomalous high Hg/TOC ratios can be used to trace large volcanism (Grasby et al., 2019). In this study, most of the cap carbonates samples show Hg/TOC ratios (~50 ppb/wt.%) that are comparable to the background Hg/TOC ratio for non-LIPs ancient carbonates (59.5 ppb/wt.%) and global marine sediments (71.9 ppb/wt.%, Grasby et al., 2019) deposited during non-LIP periods. Only three cap carbonates in the Wanshan sections show elevated Hg/TOC ratios of > 100 ppb/wt.%, which may be explained by their low TOC values and/or local reduced condition (Shen et al., 2022).

The lack of widespread Hg/TOC peaks in the Ediacaran cap carbonates suggest overall low levels of regional volcanic activity during the Marinoan deglaciation. This is consistent with there being no known LIP eruption during that time except for Lan et al. (2022), which proposed that prolonged magmatic activity during 641–637 Ma may have shortened the Marinoan Ice Age. In this case, our results support the earlier hypothesis that the Marinoan deglaciation was triggered by global warming caused by the buildup of CO_2 emitted by the continuous background volcanism during the Marinoan Ice Age (Kirschvink, 1992; Hoffman et al., 1998). The Cryogenian Ice Age was dominated by the breakup of the Rodinia supercontinent and following the amalgamation of the Gondwana supercontinent (Cawood et al., 2016; Merdith et al., 2017). Long-lasting subduction-related magmatism would have occurred in the collision of Gondwana continental fragments during the Marinoan Ice Age (Merdith et al., 2017), although we acknowledge the duration of the Marinoan Ice Age (6 to 15 Ma, Bao et al., 2018; Gong et al., 2021) is shorter than that of the subduction-related magmatism during the collision of Gondwana continental fragments. This continuous background volcanic activity would emit a substantial amount of CO_2 and Hg into the atmosphere. The emitted CO_2 would have accumulated in the atmosphere, building to a tipping point that triggered global warming and the Marinoan deglaciation (Kirschvink, 1992; Hoffman et al., 1998). The released Hg, due to its short residence time (0.5 to 2 years) in the atmosphere, would have been deposited into the ocean (Grasby et al., 2020) and evenly buried in glacial deposits during the Marinoan Ice Age, explaining the lack of Hg anomalies in the Marinoan cap carbonates.

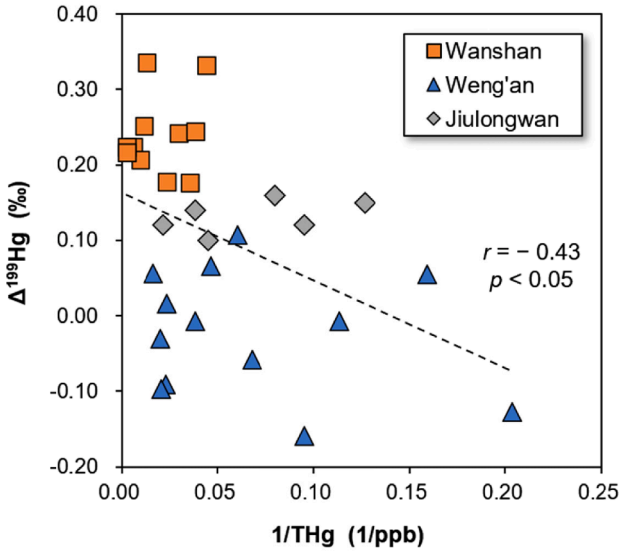

Fig. 5. The relationship between THg concentration and Δ^{199}Hg values in the studied sections. The r and p values are calculated from all three sections. The data of the Jiulongwan section are from Fan et al. (2020).

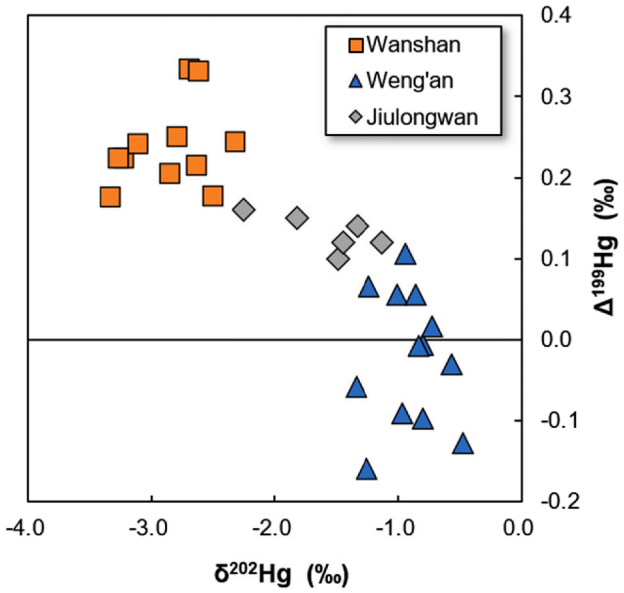

Fig. 6. Plot of Δ^{199}Hg versus δ^{202}Hg in the cap carbonates of the studied sections. The data of the Jiulongwan section are from Fan et al. (2020).

5.3. Mixing of seawater- and terrestrial-derived Hg in Ediacaran cap carbonates

Mercury isotopes provide insight into the sources of Hg in sediments. The negative δ^{202}Hg values of the studied Ediacaran cap carbonates fall into the range of that is reported for global marine sediments (−3.02 to 0.23 ‰, Blum et al., 2014; Grasby et al., 2019; Yin et al., 2017). However, the variation of Hg-MDF can result from various geochemical processes. Below we use Hg-MIF signals to trace the source of Hg in our samples. As shown in Fig. 5, THg and Δ^{199}Hg values of cap carbonates demonstrate a decreasing pattern from the Wanshan section (THg: 22.7 to 405 ppb; Δ^{199}Hg: 0.18 to 0.34 ‰), to the Weng'an section (THg: 4.91 to 61.8 ppb; Δ^{199}Hg: −0.16 to 0.11 ‰) and continuing to the Jiulongwan section (THg: 7.9 to 46.5 ppb; Δ^{199}Hg: 0.10 to 0.16 ‰). A negative correlation can be observed between Δ^{199}Hg and 1/THg (r = − 0.43, p < 0.05), possibly suggesting a binary mixing of Hg from

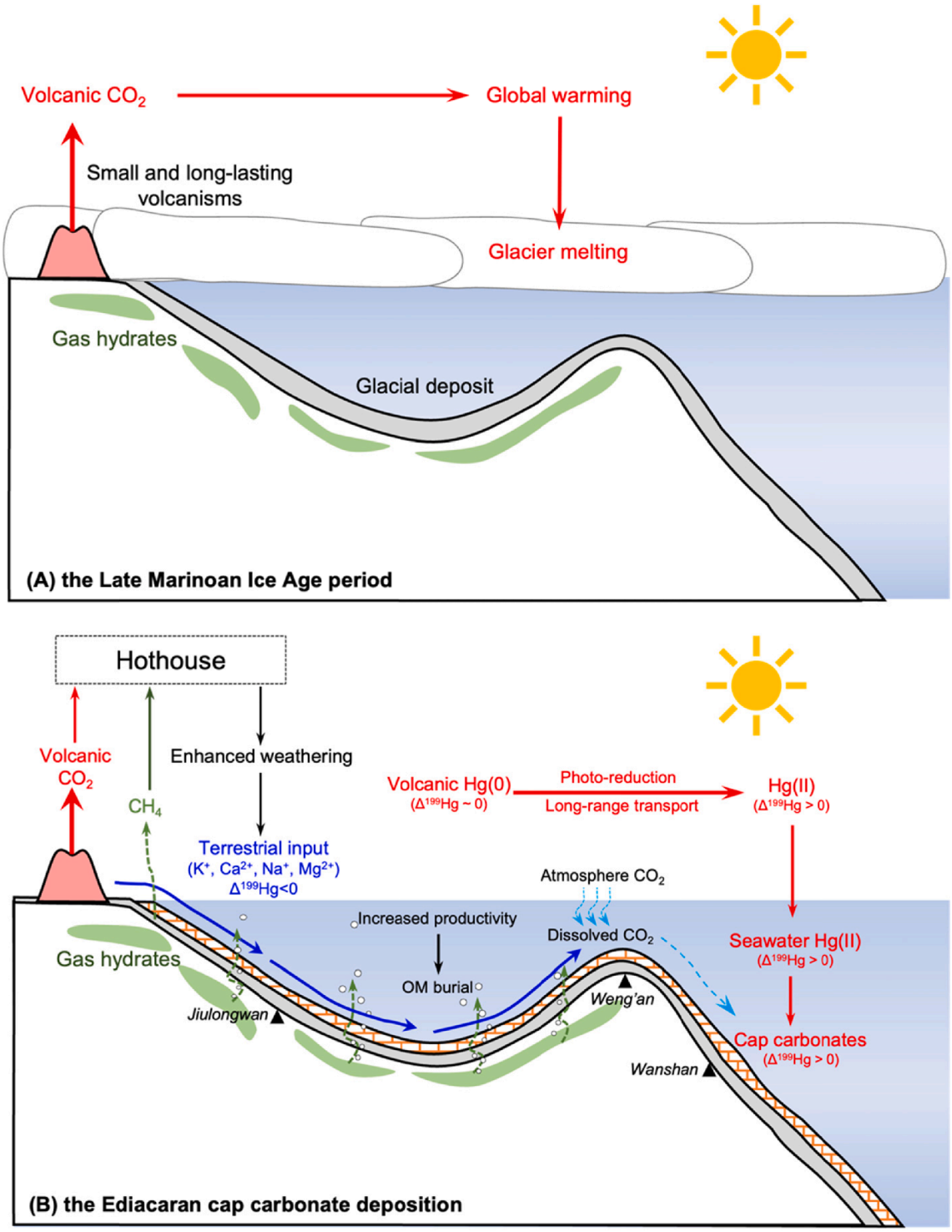

Fig. 7. Scenarios of Hg cycling during (A) the Late Marinoan Ice Age period and (B) the Ediacaran cap carbonate deposition. The sketch is not to scale.

seawater- and terrestrial-derived sources. In the $\delta^{202}Hg$-$\Delta^{199}Hg$ diagram (Fig. 6), the Jiulongwan section appears to show a mixing of Hg from two sources. The positive $\Delta^{199}Hg$ values in the Wanshan slope section are comparable to that reported for modern seawater (0.1 to 0.4 ‰, Štrok et al., 2015), suggesting a dominance of seawater Hg deposition. The relatively lower $\Delta^{199}Hg$ values in shelf sections (Weng'an and Jiulongwan) could be attributed to enhanced terrestrial input, given terrestrial systems (e.g., soil) have negative $\Delta^{199}Hg$ values (Blum et al., 2014). Plants preferentially uptake atmospheric Hg(0) into the soil, resulting in negative $\Delta^{199}Hg$ values in terrestrial material (Biswas et al., 2008; Yin et al., 2013). A recent study by Žárský et al. (2022) demonstrated the expansion of the first terrestrial flora during the Cryogenian interglacial, which may support the presence of terrestrial soil with negative $\Delta^{199}Hg$ values in the Precambrian.

6. Implications for the genesis of Ediacaran cap carbonates

The negative Ce_{anom} values in our samples, which are indicative of oceanic oxic conditions, are in line with the negative $\delta^{13}C_{carb}$ excursion in Ediacaran cap carbonates due to the oxidation of dissolved organic

matter (DOM) in deeper seawater (Kennedy et al., 2001; Shield et al., 2019; Chen et al., 2021). The Hg data in our study provide further insight into the genesis of Ediacaran cap carbonates, as shown in Fig. 7 and discussed below.

Continuous magmatism, due to the final stages of the breakup of supercontinent Rodinia during the late stage of Marinoan Ice Age (Merdith et al., 2017), would have slowly released CO_2 into the atmosphere and gradually increased atmospheric CO_2 to a tipping point that triggered global warming and melting of sea ice cover. As sea ice was melted, the global ocean warmed up to a point to then trigger the destabilization of gas hydrates (methane) in the ocean, causing the release of methane, an even more efficient greenhouse gas than CO_2, into the atmosphere, pushing global temperature to higher levels (Ruppel and Kessler, 2017).

High atmospheric CO_2 level during the Marinoan deglaciation would have had profound consequences on the land–ocean system. Not only would it have increased the dissolved CO_2 level (as HCO_3^-) in seawater due to the melting of sea ice cover but also facilitated chemical weathering of continents, by which large amounts of alkalis (e.g., K^+, Na^+, Ca^{2+}, Mg^{2+}) would have been released from terrestrial materials and entered the ocean (Hoffman et al., 2011). In shelf or slope settings, the abundant HCO_3^-, along with large inputs of terrestrial $Ca^{2+}$and Mg^{2+}, would have resulted in extensive deposition of Ediacaran cap carbonates. In the early Ediacaran Ocean, driven by global warming, oceanic productivity would be enhanced, forming organic particles that could scavenge Hg from seawater, as indicated by the largest positive Δ^{199}Hg values being in the Wanshan slope section. Enhanced continental weathering also transported large amounts of terrestrial-derived Hg to the Ediacaran cap carbonates, as supported by the less positive to negative shifts of Δ^{199}Hg in the Jiulongwan and Weng'an shelf sections. Enhanced deposition of seawater-derived Hg and terrestrial-derived Hg explains the higher THg levels of Ediacaran cap carbonates than non-LIPs carbonates.

CRediT authorship contribution statement

Ruiyang Sun: Data curation, Investigation, Writing – original draft. **Jun Shen:** Supervision. **Stephen E. Grasby:** Conceptualization, Methodology, Supervision. **Jiawei Zhang:** Data curation, Investigation. **Jianshu Chen:** Data curation, Investigation. **Chuang Yang:** Data curation, Investigation. **Runsheng Yin:** Conceptualization, Methodology, Supervision, Writing – original draft.

Declaration of Competing Interest

The authors declare that they have no known competing financial interests or personal relationships that could have appeared to influence the work reported in this paper.

Data availability

Data will be made available on request.

Acknowledgements

This work was supported by the Natural Science Foundation of China (41873047).

Appendix A. Supplementary data

Supplementary data to this article can be found online at https://doi.org/10.1016/j.precamres.2022.106891.

References

Bao, X., Zhang, S., Jiang, G., Wu, H., Li, H., Wang, X., An, Z., Yang, T., 2018. Cyclostratigraphic constraints on the duration of the Datangpo Formation and the onset age of the Nantuo (Marinoan) glaciation in South China. Earth Planet. Sci. Lett. 483, 52–63.

Benigno, A.P.A., Saraiva, A.Á.F., Sial, A.N., Lacerda, L.D., 2021. Mercury chemostratigraphy as a proxy of volcanic-driven environmental changes in the Aptian-Albian transition, Araripe Basin, northeastern Brazil. J. South Am. Earth Sci. 107, 103020.

Biswas, A., Blum, J.D., Bergquist, B.A., Keeler, G.J., Xie, Z., 2008. Natural Mercury Isotope Variation In Coal Deposits And Organic Soils. Environ. Sci. Technol. 42, 8303–8309.

Blum, J.D., Bergquist, B.A., 2007. Reporting of variations in the natural isotopic composition of mercury. Anal Bioanal Chem 388, 353–359.

Blum, J.D., Sherman, L.S., Johnson, M.W., 2014. Mercury Isotopes in Earth and Environmental Sciences. Annu. Rev. Earth Planet. Sci. 42, 249–269.

Cawood, P.A., Strachan, R.A., Pisarevsky, S.A., Gladkochub, D.P., Murphy, J.B., 2016. Linking collisional and accretionary orogens during Rodinia assembly and breakup: Implications for models of supercontinent cycles. Earth Planet. Sci. Lett. 449, 118–126.

Charbonnier, G., Morales, C., Duchamp-Alphonse, S., Westermann, S., Adatte, T., Föllmi, K.B., 2017. Mercury enrichment indicates volcanic triggering of Valanginian environmental change. Sci. Rep. 7, 40808.

Chen, B., Hu, C., Mills, B.J.W., He, T., Andersen, M.B., Chen, X., Liu, P., Lu, M., Newton, R.J., Poulton, S.W., Shields, G.A., Zhu, M., 2021. A short-lived oxidation event during the early Ediacaran and delayed oxygenation of the Proterozoic ocean. Earth Planet. Sci. Lett. 577, 117274.

Condon, D., Zhu, M., Bowring, S., Wang, W., Yang, A., Jin, Y., 2005. U-Pb ages from the Neoproterozoic Doushantuo Formation, China. Science 308, 95–98.

Deng, C., Sun, G., Rong, Y., Sun, R., Sun, D., Lehmann, B., Yin, R., 2021. Recycling of mercury from the atmosphere-ocean system into volcanic-arc–associated epithermal gold systems. Geology 49, 309–313.

Fairchild, I.J., Fleming, E.J., Bao, H., Benn, D.I., Boomer, I., Dublyansky, Y.V., Halverson, G.P., Hambrey, M.J., Hendy, C., McMillan, E.A., Spötl, C., Stevenson, C.T. E., Wynn, P.M., 2016. Continental carbonate facies of a Neoproterozoic panglaciation, north-east Svalbard. Sedimentology 63, 443–497.

Fan, H., Fu, X., Ward, J.F., Yin, R., Wen, H., Feng, X., 2020. Mercury isotopes track the cause of carbon perturbations in the Ediacaran ocean. Geology 49, 248–252.

Font, E., Adatte, T., Sial, A.N., Drude de Lacerda, L., Keller, G., Punekar, J., 2016. Mercury anomaly, Deccan volcanism, and the end-Cretaceous mass extinction. Geology 44, 171–174.

Font, E., Chen, J., Regelous, M., Regelous, A., Adatte, T., 2021. Volcanic origin of the mercury anomalies at the Cretaceous-Paleogene transition of Bidart, France. Geology 50, 142–146.

Gong, Z., 2021. Cyclostratigraphy of the Cryogenian Fiq Formation, Oman and its implications for the age of the Marinoan glaciation. Global Planet. Change 204, 103584.

Gong, Q., Wang, X., Zhao, L., Grasby, S.E., Chen, Z.-Q., Zhang, L., Li, Y., Cao, L., Li, Z., 2017. Mercury spikes suggest volcanic driver of the Ordovician-Silurian mass extinction. Sci. Rep. 7, 5304.

Grasby, S.E., Shen, W., Yin, R., Gleason, J.D., Blum, J.D., Lepak, R.F., Hurley, J.P., Beauchamp, B., 2017. Isotopic signatures of mercury contamination in latest Permian oceans. Geology 45, 55–58.

Grasby, S.E., Them, T.R., Chen, Z., Yin, R., Ardakani, O.H., 2019. Mercury as a proxy for volcanic emissions in the geologic record. Earth-Sci. Rev. 196, 102880.

Grasby, S.E., Liu, X., Yin, R., Ernst, R.E., Chen, Z., 2020. Toxic mercury pulses into late Permian terrestrial and marine environments. Geology 48, 830–833.

Haskin, L. A., Haskin, M. A., Frey, F. A., Wildeman, T. R., 1968. Relative and Absolute Terrestrial Abundances of the Rare Earths. In L. H. Ahrens (Ed.), Origin and Distribution of the Elements Pergamon Press, pp. 889–912.

Hoffman, P.F., 1998. A Neoproterozoic Snowball Earth. Science 281, 1342–1346.

Hoffman, P.F., 2011. Strange bedfellows: glacial diamictite and cap carbonate from the Marinoan (635 Ma) glaciation in Namibia: Strange bedfellows. Sedimentology 58, 57–119.

Hoffman, P.F., et al., 2017. Snowball Earth climate dynamics and Cryogenian geology-geobiology. Sci. Adv. 3, e1600983.

Hoffman, P.F., Macdonald, F.A., Halverson, G.P., 2011. Chemical sediments associated with Neoproterozoic glaciation: iron formation, cap carbonate, barite and phosphorite. In: Arnaud, E., Halverson, G.P., Shields-Zhou, G. (Eds.), The Geological Record of Neoproterozoic Glaciations. 36. Geological Society of London Memoir, pp.67–80.

Hu, D., Li, M., Chen, J., Luo, Q., Grasby, S.E., Zhang, T., Yuan, S., Xu, Y., Finney, S.C., Sun, L., Shen, Y., 2021. Major volcanic eruptions linked to the Late Ordovician mass extinction: Evidence from mercury enrichment and Hg isotopes. Global Planet. Change 196, 103374.

Huang, Y., Chen, Z.-Q., Wignall, P.B., Grasby, S.E., Zhao, L., Wang, X., Kaiho, K., 2018. Biotic responses to volatile volcanism and environmental stresses over the Guadalupian-Lopingian (Permian) transition. Geology 47, 175–178.

Hyde, W.T., Crowley, T.J., Baum, S.K., Peltier, W.R., 2000. Neoproterozoic "snowball Earth" simulations with a coupled climate/ice-sheet model. Nature 405, 425–429.

Jiang, G., Kennedy, M.J., Christie-Blick, N., 2003. Stable isotopic evidence for methane seeps in Neoproterozoic postglacial cap carbonates. Nature 426, 822–826.

Jiang, G., Shi, X., Zhang, S., 2006. Methane seeps, methane hydrate destabilization, and the late Neoproterozoic postglacial cap carbonates. Chin. Sci. Bull. 51, 1152–1173.

Jiang, G., Shi, X., Zhang, S., Wang, Y., Xiao, S., 2011. Stratigraphy and paleogeography of the Ediacaran Doushantuo Formation (ca. 635–551Ma) in South China. Gondwana Res. 19, 831–849.
Jones, D.S., Martini, A.M., Fike, D.A., Kaiho, K., 2017. A volcanic trigger for the Late Ordovician mass extinction? Mercury data from south China and Laurentia. Geology 45, 631–634.
Kaiho, K., Aftabuzzaman, M.d., Jones, D.S., Tian, L., 2020. Pulsed volcanic combustion events coincident with the end-Permian terrestrial disturbance and the following global crisis. Geology 49, 289–293.
Kennedy, M.J., Christie-Blick, N., Sohl, L.E., 2001. Are Proterozoic cap carbonates and isotopic excursions a record of gas hydrate destabilization following Earth's coldest intervals? Geology 29, 443–446.
Kennedy, M., Mrofka, D., von der Borch, C., 2008. Snowball Earth termination by destabilization of equatorial permafrost methane clathrate. Nature 453, 642–645.
Kirschvink, J.L., 1992. Late Proterozoic Low-Latitude Global Glaciation: the Snowball Earth. In: Schopf, J.W., Klein, C. (Eds.), The Proterozoic Biosphere. Cambridge University Press, Cambridge, pp. 51–52.
Knoll, A.H., Bambach, R.K., Canfield, D.E., Grotzinger, J.P., 1996. Comparative Earth History and Late Permian Mass Extinction. Science 273, 452–457.
Kwon, S.Y., Blum, J.D., Yin, R., Tsui, M.T.K., Yang, Y.H., Choi, J.W., 2020. Mercury stable isotopes for monitoring the effectiveness of the Minamata Convention on Mercury. Earth-Sci. Rev. 203, 103111.
Lan, Z., Huyskens, M.H., Le Hir, G., Mitchell, R.N., Yin, Q., Zhang, G., Li, X., 2022. Massive Volcanism May Have Foreshortened the Marinoan Snowball Earth. Geophys. Res. Lett. 49 e2021GL097156.
Lang, X., Shen, B., Peng, Y., Xiao, S., Zhou, C., Bao, H., Kaufman, A.J., Huang, K., Crockford, P.W., Liu, Y., Tang, W., Ma, H., 2018. Transient marine euxinia at the end of the terminal Cryogenian glaciation. Nat. Commun. 9, 3019.
Liang, Q., Jing, H., Conrad, D.G., 2000. Determination of trace elements in granites by inductively coupled plasma mass spectrometry. Talanta 51, 507–513.
McLennan, S.M., 1989. Rare earth elements in sedimentary rocks; influence of provenance and sedimentary processes. Rev. Mineral. 21, 169–200.
Merdith, A.S., Collins, A.S., Williams, S.E., Pisarevsky, S., Foden, J.D., Archibald, D.B., Blades, M.L., Alessio, B.L., Armistead, S., Plavsa, D., Clark, C., Müller, R.D., 2017. A full-plate global reconstruction of the Neoproterozoic. Gondwana Res. 50, 84–134.
Meyer, K.W., Petersen, S.V., Lohmann, K.C., 2019. Biogenic carbonate mercury and marine temperature records reveal global influence of Late Cretaceous Deccan Traps. Nat. Commun. 10, 5356.
Meyer, E.E., Quicksall, A.N., Landis, J.D., Link, P.K., Bostick, B.C., 2012. Trace and rare earth elemental investigation of a Sturtian cap carbonate, Pocatello, Idaho: Evidence for ocean redox conditions before and during carbonate deposition. Precambrian Res. 192–195, 89–106.
Myrow, P.M., Lamb, M.P., Ewing, R.C., 2018. Rapid sea level rise in the aftermath of a Neoproterozoic snowball Earth. Science 360, 649–651.
Percival, L.M.E., Witt, M.L.I., Mather, T.A., Hermoso, M., Jenkyns, H.C., Hesselbo, S.P., Al-Suwaidi, A.H., Storm, M.S., Xu, W., Ruhl, M., 2015. Globally enhanced mercury deposition during the end-Pliensbachian extinction and Toarcian OAE: A link to the Karoo-Ferrar Large Igneous Province. Earth Planet. Sci. Lett. 428, 267–280.
Pruss, S.B., Jones, D.S., Fike, D.A., Tosca, N.J., Wignall, P.B., 2019. Marine anoxia and sedimentary mercury enrichments during the Late Cambrian SPICE event in northern Scotland. Geology 47, 475–478.
Racki, G., 2020. A volcanic scenario for the Frasnian-Famennian major biotic crisis and other Late Devonian global changes: More answers than questions? Global Planet. Change 189, 103174.
Racki, G., Rakociński, M., Marynowski, L., Wignall, P.B., 2018. Mercury enrichments and the Frasnian-Famennian biotic crisis: A volcanic trigger proved? Geology 46, 543–546.
Rakociński, M., Pisarzowska, A., Corradini, C., Narkiewicz, K., Dubicka, Z., Abdiyev, N., 2021. Mercury spikes as evidence of extended arc-volcanism around the Devonian-Carboniferous boundary in the South Tian Shan (southern Uzbekistan). Sci. Rep. 11, Art. no. 1.
Ruppel, C.D., Kessler, J.D., 2017. The interaction of climate change and methane hydrates. Rev. Geophys. 55, 126–168.
Sanei, H., Grasby, S.E., Beauchamp, B., 2012. Latest Permian mercury anomalies. Geology 40, 63–66.
Sansjofre, P., Ader, M., Trindade, R.I.F., Elie, M., Lyons, J., Cartigny, P., Nogueira, A.C. R., 2011. A carbon isotope challenge to the snowball Earth. Nature 478, 93–96.
Scaife, J.D., Ruhl, M., Dickson, A.J., Mather, T.A., Jenkyns, H.C., Percival, L.M.E., Hesselbo, S.P., Cartwright, J., Eldrett, J.S., Bergman, S.C., Minisini, D., 2017. Sedimentary Mercury Enrichments as a Marker for Submarine Large Igneous Province Volcanism? Evidence From the Mid-Cenomanian Event and Oceanic Anoxic Event 2 (Late Cretaceous). Geochem. Geophys. Geosyst. 18, 4253–4275.
Schumacher, B., 2002. Methods for the Determination of Total Organic Carbon (TOC) In Soils and Sediments. Ecological Risk Assessment Support Center Office of Research and Development.
Selin, N.E., 2009. Global Biogeochemical Cycling of Mercury: A Review. Annu. Rev. Environ. Resour. 34, 43–63.
Shen, J., Algeo, T.J., Planavsky, N.J., Yu, J., Feng, Q., Song, H., Song, H., Rowe, H., Zhou, L., Chen, J., 2019a. Mercury enrichments provide evidence of Early Triassic volcanism following the end-Permian mass extinction. Earth-Sci. Rev. 195, 191–212.
Shen, J., Chen, J., Algeo, T.J., Yuan, S., Feng, Q., Yu, J., Zhou, L., O'Connell, B., Planavsky, N.J., 2019b. Evidence for a prolonged Permian-Triassic extinction interval from global marine mercury records. Nat. Commun. 10, 1563.
Shen, J., Feng, Q., Algeo, T.J., Liu, J., Zhou, C., Wei, W., Liu, J., Them, T.R., Gill, B.C., Chen, J., 2020. Sedimentary host phases of mercury (Hg) and implications for use of Hg as a volcanic proxy. Earth Planet. Sci. Lett. 543, 116333.
Shen, J., Yin, R., Zhang, S., Algeo, T.J., Bottjer, D.J., Yu, J., Xu, G., Penman, D., Wang, Y., Li, L., Shi, X., Planavsky, N.J., Feng, Q., Xie, S., 2022. Intensified continental chemical weathering and carbon-cycle perturbations linked to volcanism during the Triassic-Jurassic transition. Nat. Commun. 13, 1–10.
Shields, G.A., 2005. Neoproterozoic cap carbonates: a critical appraisal of existing models and the plumeworld hypothesis. Terra Nova 17, 299–310.
Shields, G.A., Mills, B.J.W., Zhu, M., Raub, T.D., Daines, S.J., Lenton, T.M., 2019. Unique Neoproterozoic carbon isotope excursions sustained by coupled evaporite dissolution and pyrite burial. Nat. Geosci. 12, 823–827.
Sial, A.N., Lacerda, L.D., Ferreira, V.P., Frei, R., Marquillas, R.A., Barbosa, J.A., Gaucher, C., Windmöller, C.C., Pereira, N.S., 2013. Mercury as a proxy for volcanic activity during extreme environmental turnover: The Cretaceous-Paleogene transition. Palaeogeogr., Palaeoclimatol. Palaeoecol. 387, 153–164.
Sial, A.N., Chen, J., Lacerda, L.D., Frei, R., Tewari, V.C., Pandit, M.K., Gaucher, C., Ferreira, V.P., Cirilli, S., Peralta, S., Korte, C., Barbosa, J.A., Pereira, N.S., 2016. Mercury enrichment and Hg isotopes in Cretaceous-Paleogene boundary successions: Links to volcanism and palaeoenvironmental impacts. Cretaceous Res. 66, 60–81.
Štrok, M., Baya, P.A., Hintelmann, H., 2015. The mercury isotope composition of Arctic coastal seawater. C.R. Geosci. 347, 368–376.
Taylor, S.R., McLennan, S.M., 1985. The continental crust: Its composition and evolution: An examination of the geochemical record preserved in sedimentary rocks. Scientific Publications, Oxford, Blackwell.
Thibodeau, A.M., Ritterbush, K., Yager, J.A., West, A.J., Ibarra, Y., Bottjer, D.J., Berelson, W.M., Bergquist, B.A., Corsetti, F.A., 2016. Mercury anomalies and the timing of biotic recovery following the end-Triassic mass extinction. Nat. Commun. 7, 11147.
Tremblin, M., Khozyem, H., Adatte, T., Spangenberg, J.E., Fillon, C., Grauls, A., Hunger, T., Nowak, A., Läuchli, C., Lasseur, E., Roig, J.-Y., Serrano, O., Calassou, S., Guillocheau, F., Castelltort, S., 2022. Mercury enrichments of the Pyrenean foreland basins sediments support enhanced volcanism during the Paleocene-Eocene thermal maximum (PETM). Global Planet. Change 212, 103794.
Wang, X., Cawood, P.A., Zhao, H., Zhao, L., Grasby, S.E., Chen, Z.-Q., Wignall, P.B., Lv, Z., Han, C., 2018. Mercury anomalies across the end Permian mass extinction in South China from shallow and deep water depositional environments. Earth Planet. Sci. Lett. 496, 159–167.
Wang, J., Jiang, G., Xiao, S., Li, Q., Wei, Q., 2008. Carbon isotope evidence for widespread methane seeps in the ca. 635 Ma Doushantuo cap carbonate in south China. Geology 36, 347–350.
Yin, R., Feng, X., Meng, B., 2013. Stable mercury isotope variation in rice plants (Oryza sativa L.) from the Wanshan mercury mining district. SW China. Environ. Sci. Technol. 47, 2238–2245.
Yin, R., Krabbenhoft, D.P., Bergquist, B.A., Zheng, W., Lepak, R.F., Hurley, J.P., 2016. Effects of mercury and thallium concentrations on high precision determination of mercury isotopic composition by Neptune Plus multiple collector inductively coupled plasma mass spectrometry. J. Anal. At. Spectrom. 31, 2060–2068.
Yin, R., Xu, L., Lehmann, B., Lepak, R.F., Hurley, J.P., Mao, J., Feng, X., Hu, R., 2017. Anomalous mercury enrichment in Early Cambrian black shales of South China: Mercury isotopes indicate a seawater source. Chem. Geol. 467, 159–167.
Yu, W., Algeo, T.J., Zhou, Q., Du, Y., Wang, P., 2020. Cryogenian cap carbonate models: a review and critical assessment. Palaeogeogr., Palaeoclimatol., Palaeoecol. 552, 109727.
Zambardi, T., Sonke, J.E., Toutain, J.P., Sortino, F., Shinohara, H., 2009. Mercury emissions and stable isotopic compositions at Vulcano Island (Italy). Earth Planet. Sci. Lett. 277, 236–243.
Žárský, J., Žárský, V., Hanáček, M., Žárský, V., 2022. Cryogenian glacial habitats as a plant terrestrialisation cradle – the origin of the anydrophytes and Zygnematophyceae split. Front. Recent Dev. Plant Sci. 735020.
Zerkle, A.L., Yin, R., Chen, C., Li, X., Izon, G.J., Grasby, S.E., 2020. Anomalous fractionation of mercury isotopes in the Late Archean atmosphere. Nat. Commun. 11, 1709.
Zhang, J., Deng, C., Liu, W., Tang, Z., Wang, Y., Ye, T., Liang, W., Liu, L., 2021. Mercury Anomalies Link to Extensive Volcanism Across the Late Devonian Frasnian-Famennian Boundary in South China. Front. Earth Sci. 9, 691827.
Zhao, H., Grasby, S.E., Wang, X., Zhang, L., Liu, Y., Chen, Z.-Q., Hu, Z., Huang, Y., 2022a. Mercury enrichments during the Carnian Pluvial Event (Late Triassic) in South China. Geol. Soc. Am. Bull. 130, 12.
Zhao, Z., Shen, B., Zhu, J.-M., Lang, X., Wu, G., Tan, D., Pei, H., Huang, T., Ning, M., Ma, H., 2021. Active methanogenesis during the melting of Marinoan snowball Earth. Nat. Commun. 12, 955.
Zhao, H., Shen, J., Algeo, T.J., Racki, G., Chen, J., Huang, C., Song, J., Qie, W., Gong, Y., 2022b. Mercury isotope evidence for regional volcanism during the Frasnian-Famennian transition. Earth Planet. Sci. Lett. 581, 117412.
Zhou, C., Huyskens, M.H., Lang, X., Xiao, S., Yin, Q.-Z., 2019. Calibrating the terminations of Cryogenian global glaciations. Geology 47, 251–254.
Zhou, T., Pan, X., Sun, R., Deng, C., Shen, J., Kwon, S.Y., Grasby, S.E., Xiao, J., Yin, R., 2021. Cryogenian interglacial greenhouse driven by enhanced volcanism: Evidence from mercury records. Earth Planet. Sci. Lett. 564, 116902.